Supplementary information

Moiré bands in twisted trilayer black phosphorene: effects of pressure and electric field

Erqing Wang[a], Xiaolong Zou[a]*

[a] Shenzhen Geim Graphene Center, Tsinghua-Berkeley Shenzhen Institute and Tsinghua Shenzhen International Graduate School, Tsinghua University, Shenzhen, 518055, China

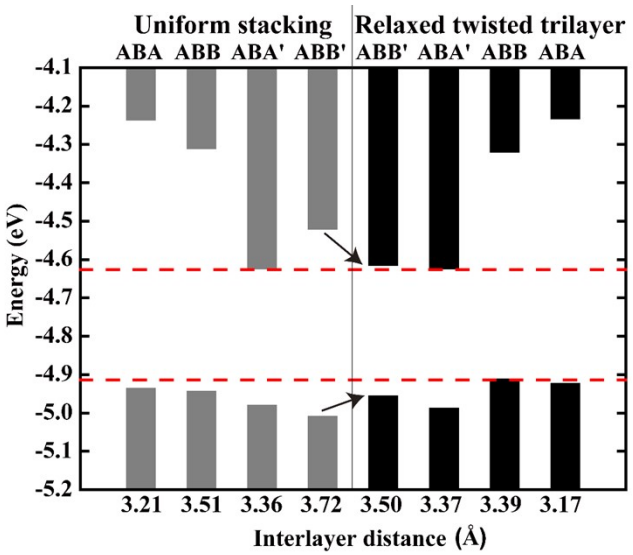

Fig. S1. The band alignment of high-symmetry stacking configurations in ABT^2, taking vacuum level as reference. The dark grey and black bars represent energy levels of different stacking configurations with interlayer distances from uniform stacking and relaxed twisted systems, respectively. The red dashed lines indicate the lowest conduction band edge and the highest valence band edge for cases with interlayer distance from relaxed ABT^2. The numbers at the horizontal axis represent the distances between the top and middle layers.

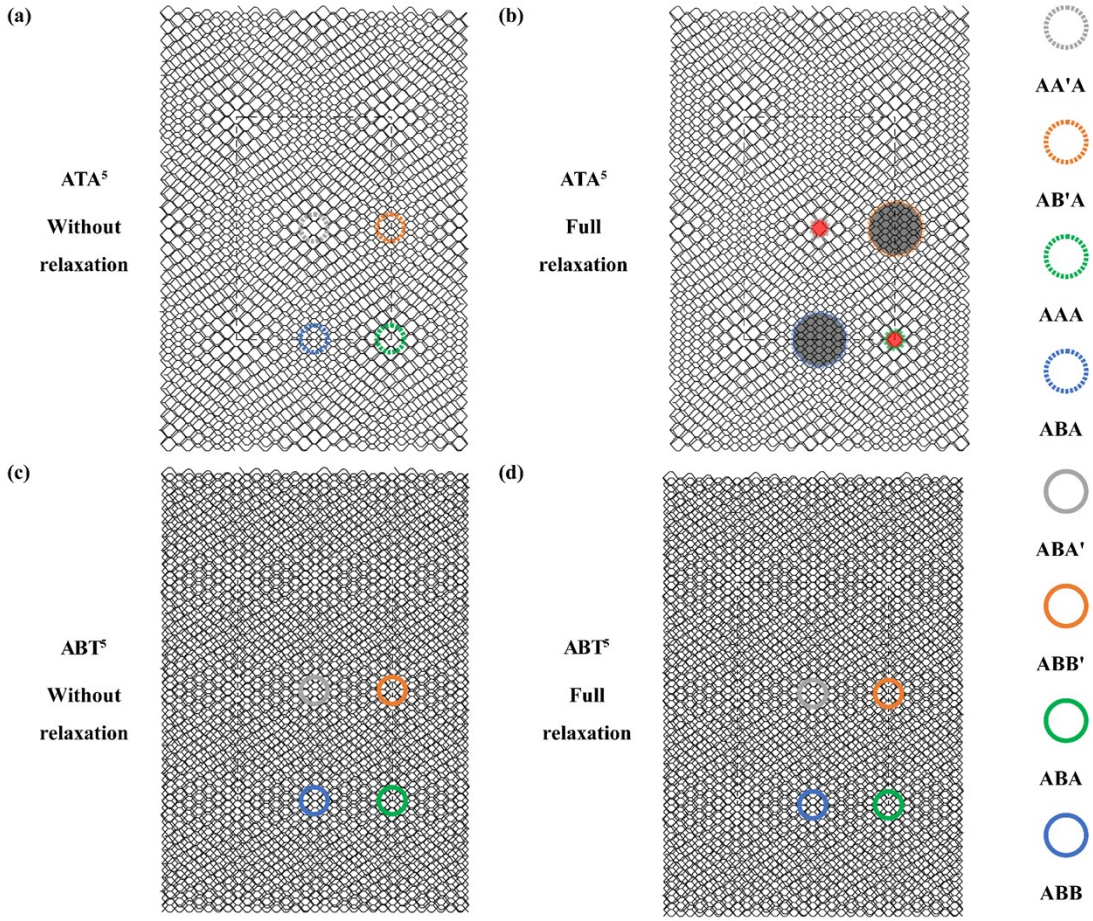

Fig. S2. The structures of (a), (c) ATA^5 and (b), (d) ABT^5 systems without and with relaxation. For ATA^5, the enlarged and shrunken areas after relaxation are shaded in black and red, respectively. In contrast, no obvious change in the areas of high-symmetry stacking configurations is observed in ABT^5.

Table S1. Calculated energies of all seven high-symmetry stacking configurations with interlayer distance from uniform stacking and relaxed 5° twisted trilayers. Energy is in the unit of eV.

High-symmetry stacking configurations	Distances from uniform stacking	Distances from Relaxed twisted ATA^5/ ABT^5
ABA	-60.89	-46.93
ABB	-60.89	-46.85
ABA'	-60.87	-46.87
ABB'	-60.88	-46.78
AA'A	-60.88	-46.62
AB'A	-60.85	-46.81
AAA	-60.89	-46.78

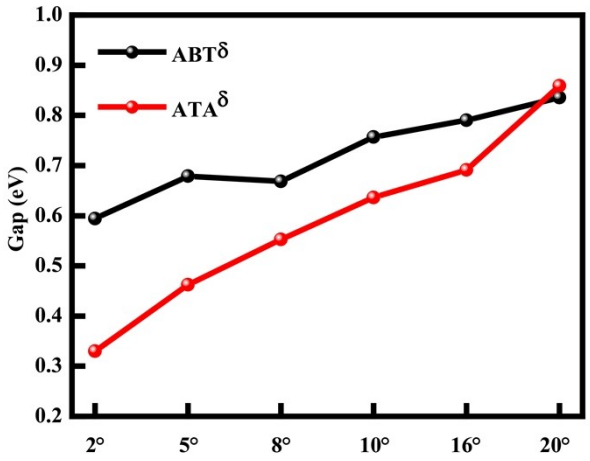

Fig. S3. The bandgap evolution in ATA^{δ} and ABT^{δ} systems. As the twist angle decreases, the bandgap of ATA^{δ} reduces much more significantly compared with ABT^{δ}.

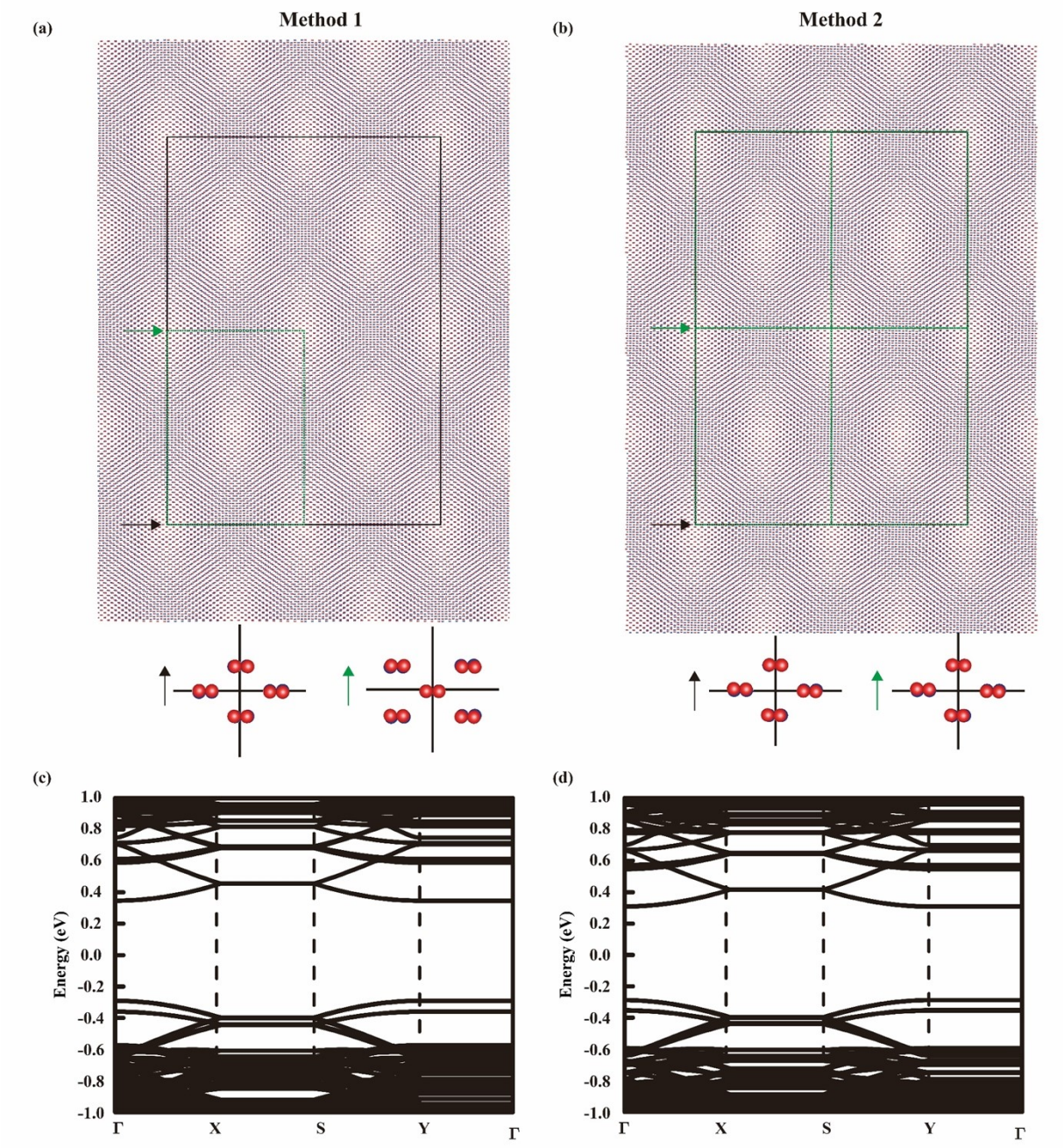

Fig. S4. (a),(b) The moiré patterns of ATA[2] system using two methods[1, 2] to construct the supercell. The green rectangles represent minimal moiré unit cells. When the supercell is constructed using the first method with two different layers rotated by +1° and -1°, two microscopically distinguishable structures with a very similar stacking configuration along one periodic direction can be identified, as shown by the local structures at the bottom panels. Accordingly, one supercell (black rectangle) contains four moiré unit cells (green rectangle). Whereas for supercell constructed using the second method with two different layers rotated by +2° and 0°, it contains one minimal moiré unit cell. The inclusion of multiple moiré unit cells in one supercell leads to the band degeneracy along X-S direction. As an example, band structures of ATA[10] system calculated using the supercells containing

four moiré unit cells constructed using both methods give similar characteristics, in particular the band degeneracy along X-S direction, as shown in (c) and (d).

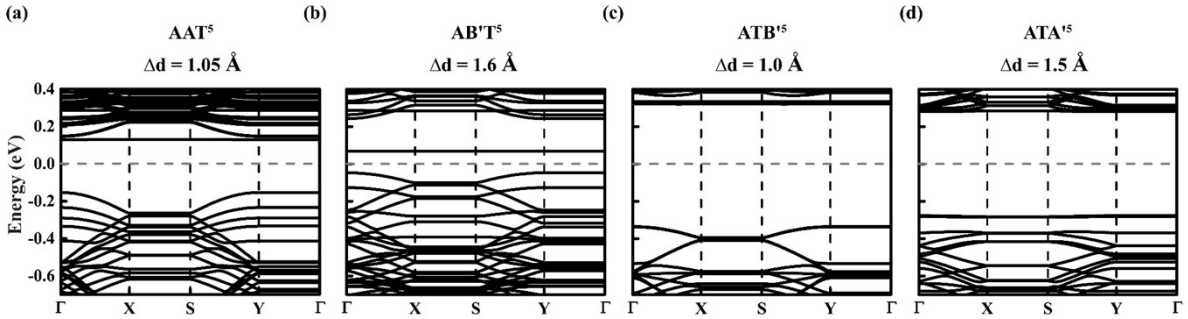

Fig. S5. Electronic structures of TTbP with twist angle 5° under pressure using mBJ functional. Δd indicates the decreased thickness in Å.

Table S2. The bandwidths of flat bands in five TTbP with twist angle 5° under certain pressure are indicated in Fig. S5†. Bandwidths is in the unit of meV.

Method	Twisting trilayer bP	Width of the flat conduction band(meV)	Width of the flat valence band (meV)
RESCU(MBJ)	ATA^5	0.55	/
	AAT^5	1.61	/
	AB'T^5	0.07	/
	ATA'^{5}	3.30	6.47
	ATB'^{5}	0.70	/

Note S1. Estimated pressure required to quasi-1D-to-0D crossover of moiré states

To estimate the required pressure to drive the crossover of moiré states, we take pristine bP as our example to investigate the connection between pressure and compressed thickness and ignore the change of in-plane lattice parameter for simplicity. As shown in Fig. S6†, the interlayer distance decreases by ~ 0.50 Å (corresponding to the decreased thickness of ~ 1.0 Å in trilayer systems) when perpendicular pressure approaches 10 GPa. Such a level of pressure can be easily achieved in layered materials.[3-6] In sharp contrast, to realize a similar crossover in twisted bilayer bP, the decrease of interlayer distance reaches 1.0 Å (Fig. S7†), which suggests a much larger pressure is required for potential experimental observation.

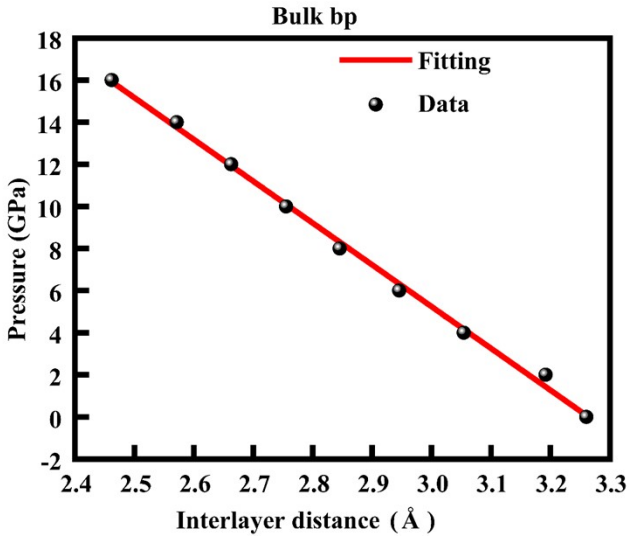

Fig. S6. The perpendicular pressure was calculated as a function of interlayer distance for the bulk black phosphorene system. The black balls and red line represent DFT's results and fitted curve, respectively.

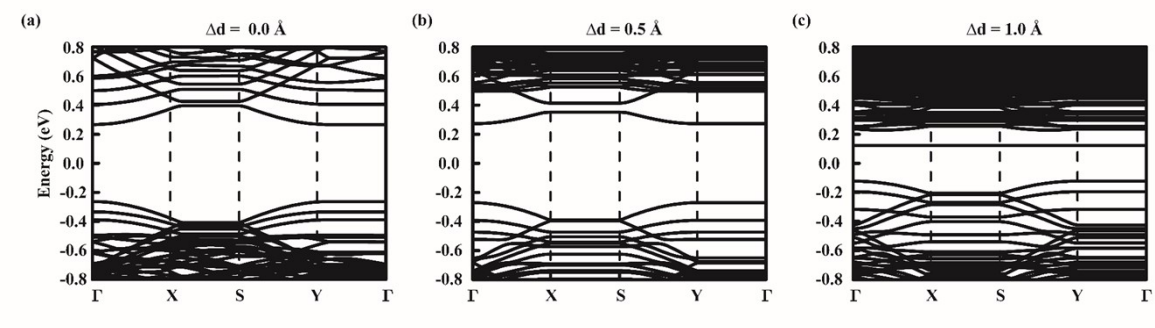

Fig. S7. Electronic structures of AT^5 under pressure using mBJ functional. The numbers are the decreased thickness in Å.

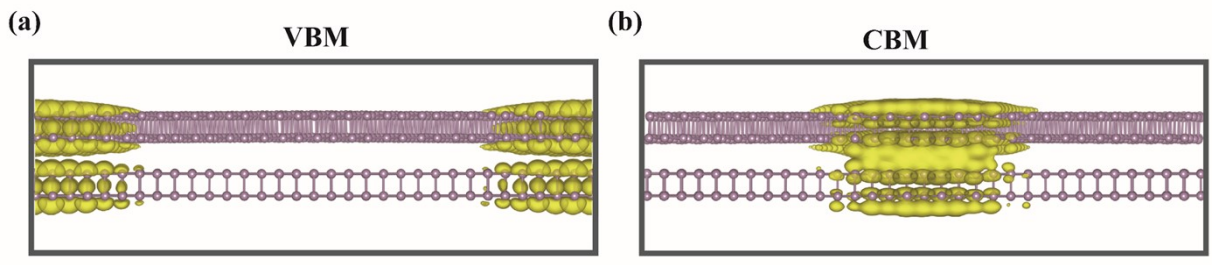

Fig. S8. The charge density distribution of VBM and CBM states in AT^5 with zero fields. The iso-surface value is set as 5×10^{-11} e $Å^{-3}$.

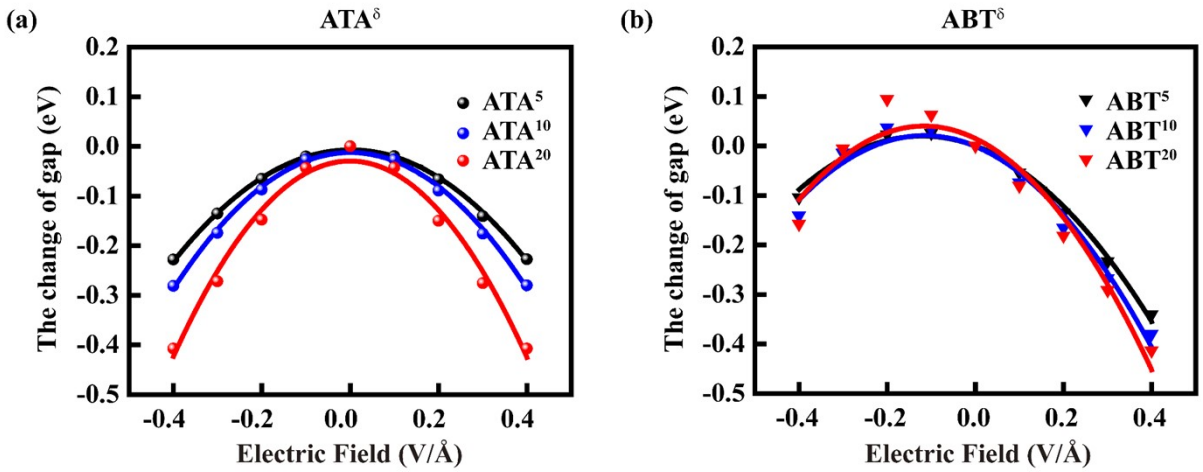

Fig. S9. (a)/(b) The change of bandgap with electric field in ATA$^{\delta}$ /ABT$^{\delta}$, with fitted results represented by lines. The black, blue, and red spheres (inverted triangle) represent ATA^{5}/ABT^{5}, ATA^{10}/ABT^{10}, and ATA^{20} /ABT^{20}, respectively.

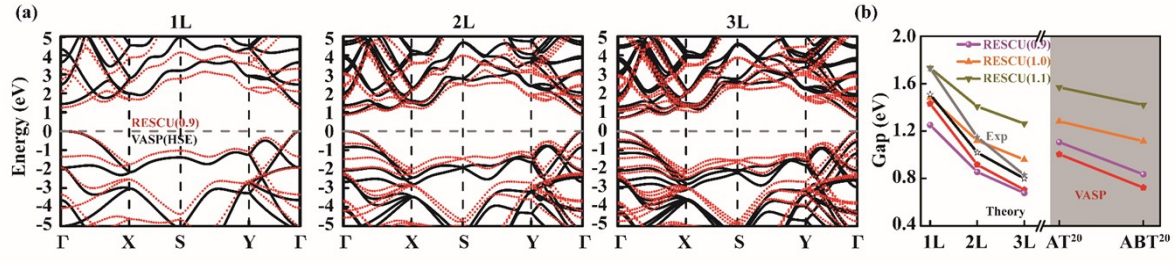

Fig. S10. (a) Electronic band structures were obtained from the mBJ method using RESCU (dashed red line) and the HSE method using VASP (solid black line) for 1L, 2L, and 3L bP. (b) The bandgap of different bP systems was obtained using different methods. The red, purple, orange, and dark yellow symbols represent our results, while grey and black ones are from experimental and theoretical references listed in Table S3. The numbers in parenthesis indicate different charge gradient parameters in the mBJ calculations.

Table S3. Calculated bandgaps of the monolayer (1L), bilayer with AB stacking, trilayer with ABA stacking, and twisted AT^{20} bilayer and ABT^{20} trilayer systems. Energy is in the unit of eV. The mbjc represents the charge gradient parameter in the mBJ calculations.

Method	mbjc	1L	2L	3L	AT^{20}	ABT^{20}
VASP(HSE)		1.43	0.92	0.71		
VASP(MBJ)	1.16				1.01	0.72
RESCU(MBJ)	0.90	1.25	0.86	0.68	1.11	0.84
RESCU(MBJ)	1.00	1.48	1.12	0.96	1.28	1.12

RESCU(MBJ)	1.10	1.73	1.41	1.26	1.57	1.42
Exp.[7]		1.73	1.15	0.83	/	/
Theory.[8] (HSE06)		1.51	1.02	0.79	/	/

We compared geometric parameters (schematics in Fig. S11) of monolayer, bilayer, trilayer black phosphorenes using VASP with van der Waals optB88-vdw functional suitable for layered materials and RESCU with different atomic orbital basis sets, including SZP with 9 orbitals (1s + 3p + 5d), and DZP with 13 orbitals (2s + 6p + 5d). The results are shown in Table S4. It can be seen that the RESCU+DZP results are very similar as those from VASP+optB88-vdw, while RESCU+SZP calculations show slight higher deviation, but in an acceptable range. The error bars using RESCU+SZP method for lattice vectors, bond length, and bond angle are about 0.07 Å, 0.09 Å, 2.5°, respectively. Regarding the energy, we compare interlayer binding energies here. Since RESCU doesn't include van der Waals interaction, the obtained binding energies are much weaker, as expected. Nevertheless, the calculated band structures using RESCU+SZP method are very close to VASP results, as shown in Fig. S10.

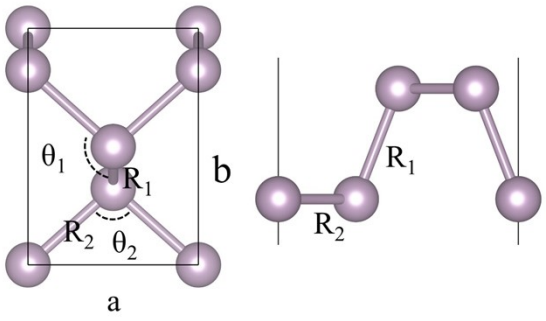

Fig. S11. Schematic top and side views of monolayer black phosphorene crystal structure. Key structural parameters, including lattice vectors (a, b), bond lengths (R_1, R_2), and bond angles (θ_1, θ_2) are indicated.

Table S4. The geometric parameters of monolayer, bilayer, and trilayer black phosphorous using VASP with optB88-vdw functional, RESCU with single-zeta basis plus polarization orbitals (SZP), and double-zeta basis plus polarization orbitals (DZP).

1L	Method	a(Å)	b(Å)	R_1(Å)	R_2(Å)	θ_1(°)	θ_2(°)	Binding Energy(eV)
VASP	optB88-vdw	3.32	4.56	2.27	2.23	103.50	95.99	/
RESCU	SZP	3.39	4.56	2.29	2.28	101.84	93.46	/
	DZP	3.31	4.53	2.28	2.22	104.02	95.87	/
2L	Method	a(Å)	b(Å)	R_1(Å)	R_2(Å)	θ_1(°)	θ_2(°)	Binding Energy(eV)
VASP	optB88-vdw	3.33	4.52	2.27	2.24	102.92	96.05	0.02

RESCU	SZP	3.39	4.57	2.31	2.33	102.37	93.94	0.01
	DZP	3.31	4.52	2.28	2.23	104.02	95.90	0.01
3L	Method	a(Å)	b(Å)	R_1(Å)	R_2(Å)	θ_1(°)	θ_2(°)	Binding Energy(eV)
VASP	optB88-vdw	3.33	4.50	2.28	2.24	102.83	96.27	0.05
RESCU	SZP	3.39	4.55	2.30	2.32	101.84	93.83	0.01
	DZP	3.30	4.53	2.30	2.23	103.01	95.68	0.02

References

1. D. Pan, T.-C. Wang, W. Xiao, D. Hu and Y. Yao, *Phys. Rev. B*, 2017, **96**, 041411.
2. P. Kang, W.-T. Zhang, V. Michaud-Rioux, X.-H. Kong, C. Hu, G.-H. Yu and H. Guo, *Phys. Rev. B*, 2017, **96**, 195406.
3. Z. Zhao, H. Zhang, H. Yuan, S. Wang, Y. Lin, Q. Zeng, G. Xu, Z. Liu, G. K. Solanki, K. D. Patel, Y. Cui, H. Y. Hwang and W. L. Mao, *Nat. Commun.*, 2015, **6**, 7312.
4. J. Xia, J. Yan, Z. Wang, Y. He, Y. Gong, W. Chen, T. C. Sum, Z. Liu, P. M. Ajayan and Z. Shen, *Nat. Phys.*, 2020, **17**, 92-98.
5. Y. Gu, S. Zhang and X. Zou, *Sci. China Mater.*, 2020, **64**, 673-682.
6. C. Zhang, Y. Gu, L. Wang, L. L. Huang, Y. Fu, C. Liu, S. Wang, H. Su, J. W. Mei, X. Zou and J. F. Dai, *Nano Lett.*, 2021, **21**, 7946-7952.
7. L. Li, J. Kim, C. Jin, G. J. Ye, D. Y. Qiu, H. Felipe, Z. Shi, L. Chen, Z. Zhang and F. Yang, *Nat. Nanotechnol.*, 2017, **12**, 21-25.
8. J. Qiao, X. Kong, Z.-X. Hu, F. Yang and W. Ji, *Nat. Commun.*, 2014, **5**, 4475.